Marine Structures 92 (2023) 103505

Contents lists available at ScienceDirect

Marine Structures

journal homepage: www.elsevier.com/locate/marstruc

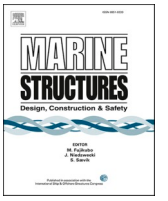

Fatigue life assessment of offshore wind support structures in the presence of corrosion pits

Muhammad Shamir [a], Jarryd Braithwaite [b], Ali Mehmanparast [a,*]

[a] Department of Naval Architecture, Ocean & Marine Engineering, University of Strathclyde, Glasgow, G1 1XQ, UK
[b] School of Aerospace, Transport, & Manufacturing, Cranfield University, MK43 0AL, Cranfield, Bedfordshire, UK

ARTICLE INFO

Keywords:
Durability
Fatigue
Pitting corrosion
S355 steel
Offshore wind turbine

ABSTRACT

Offshore wind turbine support structures, which connect the wind turbine transition piece and/or tower to the seabed, are located below the sea level and are in direct contact with seawater during the entire lifespan; therefore, they are highly susceptible to corrosion damage and cracking. In particular, the pitting corrosion is very crucial in these support structures, as it leads to local stress concentrations and thus affects the fatigue life. Although corrosion protection mechanisms are commonly implemented in offshore wind turbines, they have a finite life and therefore corrosion damage cannot be completely avoided during the entire life cycle, and this can lead to pitting corrosion on the steel surface. This paper aims to investigate the impact of pitting corrosion on fatigue durability of steel structures by performing tests on lab-scale coupons, made of S355 structural steel which is widely employed in fabrication of offshore wind support structures. For this purpose, cross-weld uniaxial samples were initially exposed to seawater for different time durations and then tested under cyclic loading condition. Furthermore, the durability analysis of corroded samples was carried out using a modified NASGRO equation. The results show that the pitting corrosion significantly reduces the fatigue life, and its level of life reduction is strongly dependent on the seawater exposure time. Moreover, the results show that employment of a linear trend for lower stress ranges would result in significant underprediction of the fatigue life, hence over-conservatism in the design life, at longer seawater exposure times.

1. Introduction

With the increase in the global energy demand, efforts have been directed towards producing clean energy from renewable energy sources while battling global warming [1]. Among renewable energy sources, offshore wind energy has gained a lot of interest due to significant reduction in levelized cost of energy (LCoE) in recent years and its potential for large-scale deployment [1,2]. A recent example of such efforts is the new offshore wind farm being constructed by Siemens Gamesa Renewable off the coast of Yorkshire, UK and believed to be the largest among the current wind farms [3]. It is estimated that this wind farm could result in powering 1.2 million households in the United Kingdom by 2024 [3]. Currently, offshore and onshore wind energy contribute to about 8.1% and 9.1% of the UK's energy generation, respectively, and subsequently the reduction of 12 million tonnes of CO_2 [4,5]. Nevertheless, being a relatively new technology as compared to fossil fuels, considerable efforts have been made towards bringing down the LCoE for offshore wind power, which would render the technology commercially competitive [1].

* Corresponding author.
E-mail address: ali.mehmanparast@strath.ac.uk (A. Mehmanparast).

https://doi.org/10.1016/j.marstruc.2023.103505
Received 23 December 2022; Received in revised form 26 July 2023; Accepted 7 August 2023
Available online 14 August 2023

Nomenclature

a	Crack length/depth
A	Cyclic fracture toughness
b	Sample width
c	Crack width
D, p	Material constants in modified Hartman-Schijve equation
E	Young's modulus
K	Stress intensity factor
ΔK	Stress intensity factor range
$K_{\max}$	Maximum stress intensity factor
K_{th}	K threshold for long crack
K_{thr}	Crack length-dependent K threshold
N	Number of cycles to failure
R	Cyclic load ratio
R^2	Coefficient of determination
S, $\Delta\sigma$	Stress range
t	Thickness of small crack sample
EIFS	Equivalent initial flaw size
LEFM	Linear elastic fracture mechanics
BM	Base metal
HAZ	Heat affected zone
WM	Weld Metal

A significant challenge in the offshore wind industry is to provide optimised design solutions and reliable assessment of structural integrity of the support structures, which subsequently impacts the LCoE of energy from offshore wind [6]. The foundation structure acts as a life-limiting component for an offshore wind turbine (OWT) as it is subjected to a spectrum of structural loads, such as weight of the rotor and nacelle assembly, bending load from wind, wave loads, current loads, and vibrations due to rotor blades [7]. The dominant majority of the installed OWTs are supported using monopile foundations which are manufactured by stacking and welding together large diameter and thickness cylindrical sections, often referred to as cans, which can cost up to 35% of the total setup cost of an OWT [8,9]. The circumferential weldments joining the thick monopile sections can lead to material property variations at the weld metal (WM)-heat affected zone (HAZ)-base metal (BM) interface where the cracks are typically found to initiate and propagate [10]. This is due to the difference in microstructure and chemical segregation resulting from rapid heating and cooling associated with the submerged arc welding process [11]. A number of studies in the literature have been carried out to evaluate the structural integrity of monopile structures fabricated using structural steels e.g. Refs. [12,13]. Jacob et al. [2] investigated the residual stress profile in a typical circumferential butt weld of OWT monopile made of S355 G10 + M and found compressive residual stresses are beneficial in fatigue life enhancement of OWTs. Jacob et al. [2] also studied the stress–strain response of different material microstructures (BM, HAZ, and WM) by performing tensile tests on cross-weld (also known as X-weld) specimens using Digital Image Correlation (DIC) technique. It was found that the three regions exhibited comparable values of tensile strength; however, the elongation to failure of the WM and HAZ was reduced by a factor of 10 with respect to the BM. As the OWT weldments are not subjected to any post-weld treatment, a combination of mechanical properties mismatch (between HAZ and the surrounding BM), residual stress, and stress concentration factor (SCF) at the weld toe makes it a potential site for fatigue crack initiation and propagation. In another study conducted by Colussi et al. [14], linear elastic fracture mechanics (LEFM) approach was employed using peak stress method while assuming weld toe as a V notch. However, Ferro et al. [15] reported that if the applied stress amplitude is such that the local stress at the weld toe is beyond the elastic limit of the material, the weld residual stresses in the plastic zone would be redistributed in the first loading cycle.

Apart from the geometric discontinuities, OWTs also experience corrosion damage during the service life which under cyclic loading condition can act as crack initiation sites by elevating local stresses and resulting in corrosion-fatigue cracking [16]. For all offshore structures, the corrosive environment significantly impacts both the crack initiation and crack propagation behaviour of the material [6] and for this purpose, the influence of corrosion damage must be examined to investigate the environmental damage effects on the fatigue life reduction of OWT foundations. Corrosion-fatigue process is initiated by the formation of localized corrosion pits at certain parts of the wind turbine structure, which are formed because of the breakdown of the thin protective layer on the surface of metals, which then develop into a critical size large enough to initiate a crack [17,18]. Pitting corrosion is generally known to be a life limiting factor on subsequent fatigue life. According to recently published research of Qvale et al. [19], where DIC was used to identify crack initiations on a few corroded specimen extracted from offshore mooring chains, the existence of corrosion pits must be comprehensively examined and considered in fatigue life analysis of offshore structures. Mehmanparast et al. [6] found that the crack propagation is two times higher in seawater than in air, hence corrosion damage is found to significantly influence the fatigue life and the corrosion-fatigue cracking behaviour of the material. Due to the acidic conditions under the rust layer, hydrogen can be produced and diffuse into the steel surface, causing embrittlement of the material which affects crack initiation as well as crack propagation [20,

21]. Li et al. [22] investigated the mechanical behaviour of low alloy mild steel G250 on specimens exposed to different acidic conditions in an immersion test and reported that with lower pH values, the ultimate strength and the corresponding strain were reduced significantly.

The primary step in understanding of the corrosion damage effects on integrity assessment of OWT structures is to explore the pitting effects on the fatigue design process by considering the *S–N* curves for structural steels in seawater. In this paper, the impact of surface geometry on the fatigue performance of structural steels has been thoroughly investigated by introducing different extents of corrosion pits into the samples prior to testing. For this purpose, a total of 24 polished and pre-corroded specimens were tested until fatigue failure occurred. The samples were immersed in artificial seawater for different time periods to simulate the corrosion damage. In addition, upon completion of the planned seawater exposure time, the specimens were scanned with a high-resolution X-ray computed tomography (XCT) to estimate the crack initiation site and this was converted by reverse engineering to an analytical model that can be used to determine stress intensity factor on the surface of the specimens. The obtained results from this study have been discussed by considering the influence of immersion time on corrosion pit formation and the subsequent effect on fatigue life reduction using lab-scale samples.

2. Material and test method

The material utilised in this study is S355 G10 + M structural steel which is commonly employed in the fabrication of OWT foundation structures and many other offshore structures. The S355 G10 + M steels plates were supplied for this project after being subjected to thermomechanical rolling process. Two 90 mm-thick hot rolled plates were then welded using submerged arc welding process as shown in Fig. 1(a). Details of the welding procedure and the mechanical properties of the welded plate can be found in a previous study by Jacob et al. [2]. It has been shown in Ref. [2] that the welded plate employed in this study had the yield stress of much greater than 355 MPa and closer to 500 MPa. Subsequently, the welded plate was sectioned into 10 mm slices, as shown in Fig. 1 (b), from which the uniaxial fatigue specimens were extracted. 24 flat dog bone samples were extracted in total from the weld region and referred to as cross-weld specimens. The samples extraction location was selected such that all three of the WM, HAZ and BM material microstructures were positioned at the centre of the specimen's gauge section (see Fig. 1(b)). This configuration allows the interface between WM, HAZ, and BM to be tested under the applied cyclic loading condition using the samples designed according to ASTM E466 (Fig. 1(c) and (d)) [23].

In order to explore the angle between the loading direction and the HAZ, the extracted slices were ground, polished and etched prior to extraction of uniaxial samples. As example of the etched surface is shown in Fig. 2. As seen in this figure, in double V-grooved multi-pass butt welded joints, the orientation of the HAZ zone changes from the top to the bottom surface. The analysis of the welded plates examined in this study shows that the top and bottom V-grooves shown in Fig. 2 are oriented at approximately 65° and 82.5°, respectively, with respect to the horizontal axis and the intersection between the top and bottom grooves appears to be almost normal to the horizontal axis. This means that depending on the exact location of the cross-weld specimens extracted from 10 mm slices of welded plate, the angle between the HAZ region and the loading direction (i.e. which is parallel to the horizontal axis) varies between 65° and 90°. The welding procedure in this study replicates the current practice in offshore wind industry, therefore the test results obtained from the cross-weld specimens would represent the material behaviour of the circumferential weldments in OWT monopile structures.

In order to introduce corrosion damage into the test specimens, artificial non-biological seawater was prepared according to ASTM D1141 [24]. 15 samples were immersed in artificial seawater for different exposure times. Prior to immersion in seawater, the gripping ends of dog bone samples were covered with a thick layer of silicon protection to avoid corrosion damage being introduced in the gripping section as shown in Fig. 3(a). The samples were then immersed for two and four months in artificial seawater as shown in

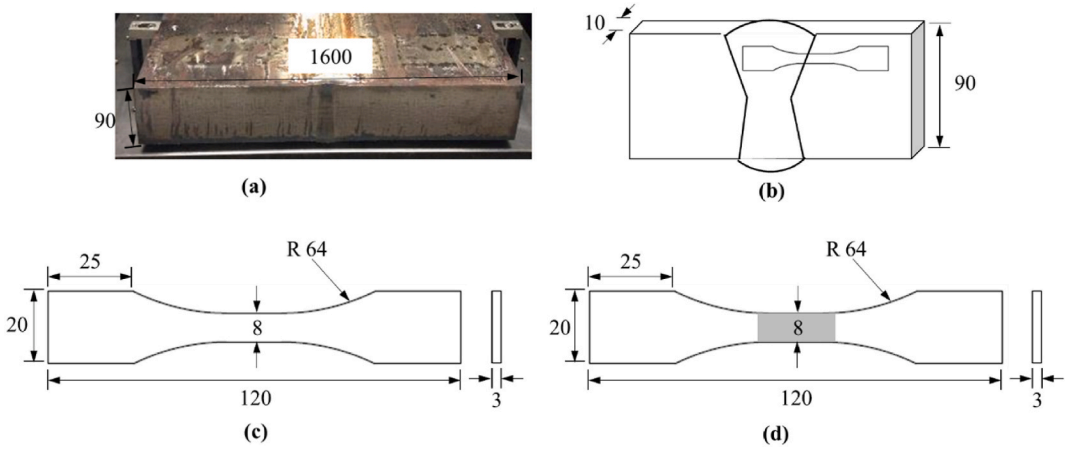

Fig. 1. (a) 90 mm thick S355 welded plate used for sample extraction, (b) schematic representation of a 10 mm slice used for fatigue sample extraction, (c) dimensions of polished samples, and (d) dimensions of pre-corroded fatigue samples (with the corroded region shaded in grey).

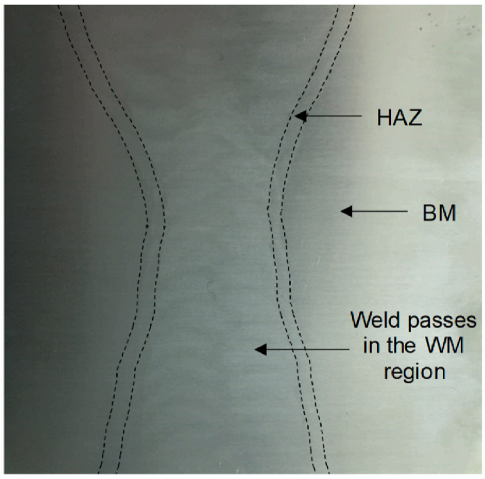

Fig. 2. Material microstructure in double V-grooved welded plate.

Fig. 3(b). After two months, 9 samples were taken out and visually observed for corrosion damage before carrying out fatigue testing, whereas the remaining 6 samples were retrieved after four months of seawater exposure. The gauge section, with the approximate length of 30 mm and width of 8 mm, of the immersed samples was covered with rust as schematically shown in Fig. 1(d) and observed in Fig. 3(c).

Once corrosion pits were introduced into the gauge region of immersed dog bone specimens, uniaxial fatigue testing was conducted on 9 uncorroded (i.e., without prior corrosion damage) specimens, 9 specimens after two months of seawater exposure and 6 specimens after four months of seawater exposure. Load controlled uniaxial fatigue testing was carried out at room temperature on a 100 kN servo-hydraulic test machine under constant amplitude sinusoidal wave loading with a load ratio of $R = P_{min}/P_{max} = 0.1$, at 20 Hz frequency as shown in Fig. 4. Before testing, the gauge section of the machined samples without prior corrosion damage was ground with appropriate sequence of sandpapers. However, for corroded samples the gauge length regions were untouched to allow the influence of pitting corrosion being examined in subsequent fatigue tests.

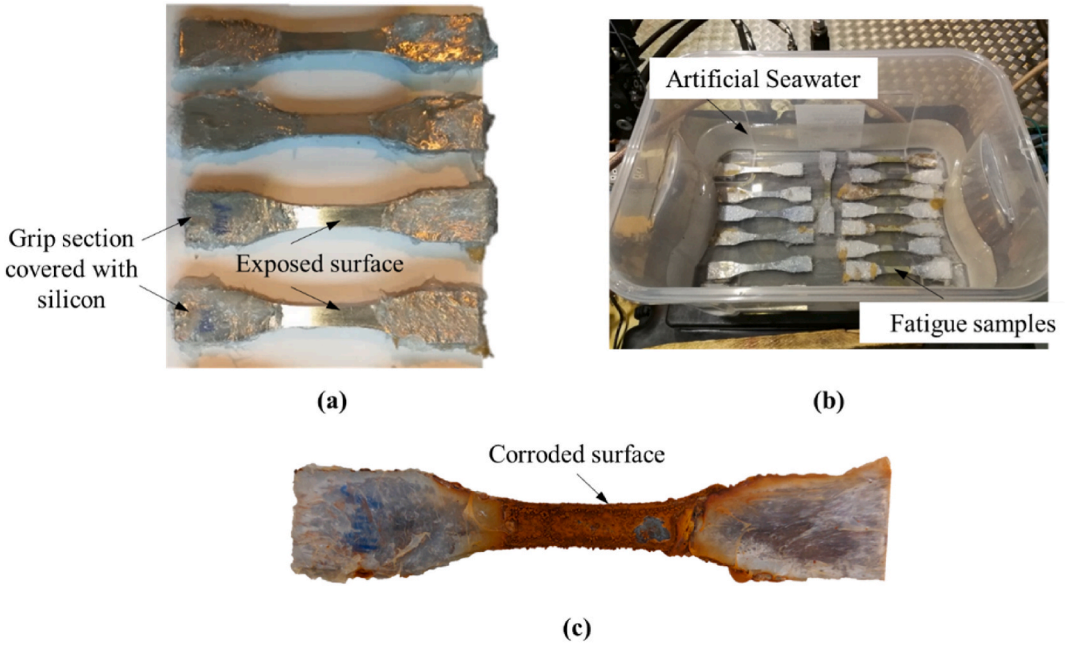

Fig. 3. (a) Fatigue samples prepared for seawater immersion, (b) illustration of fatigue samples fully immersed in artificial seawater, (c) an example of a corroded sample after seawater exposure.

Fig. 4. Illustration of the fatigue testing using a 100 kN servo-hydraulic machine.

3. Results and discussion

3.1. Pitting corrosion effects on fatigue life

The stress-life data, often referred to as *S–N* curve for design purposes where *S* is the stress range and *N* is the number of cycles to failure, obtained from uniaxial fatigue tests on corroded and uncorroded samples are presented in log-log axes in Fig. 5. In this graph, the uncorroded, 2-months corroded, and 4-months corroded cross-weld test data are shown in black, grey, and white triangles, respectively. Also included in this figure are the lines of best fit (i.e. mean curve) made to each of the three test data sets. It can be observed in Fig. 5 that for a given value of stress range the *S–N* fatigue trend from uncorroded test data falls further on the right-hand side of the graph (Fig. 4), indicating considerably higher fatigue life in the absence of corrosion pits. On the other hand, the trends obtained from corroded specimens show significantly lower fatigue life in the presence of corrosion pits, with the highest fatigue life reduction observed in specimens with four months of seawater exposure, while the data with two months of seawater exposure fall in between uncorroded and four-months corroded trends. In general, the fatigue life reduction in the presence of corrosion pits can be explained by the fact that the corroded samples were dominated by crack growth from the existing pits, whereas the uncorroded samples were dominated by crack initiation. Also seen in Fig. 5 is that within the inherent experimental scatter, all three data sets have exhibited similar slopes indicating that in addition to lower fatigue life in corroded samples the indicative endurance limit would be also lower in the presence of corrosion pits compared to uncorroded condition. The reduced fatigue life and endurance limit in corroded samples are due to the stress concentrations arising from the corrosion pits, which resulted in crack nucleation at a much smaller number of fatigue cycles. It's worth noting that while the fatigue tests in air on corroded samples might exhibit an endurance limit at low stress range levels, in most standards it is recommended to assume that no endurance limit will be observed under corrosion-fatigue condition (i.e. fatigue in free-corrosion environment) where the sample is immersed in seawater and cycled at the same time. In other words, the combination of corrosion and fatigue in a single test may result in no fatigue endurance limit, while inducing corrosion pits into the sample followed by fatigue testing in air (hence introducing corrosion and fatigue in isolation from each other) may lead to a different observation in terms of endurance limit.

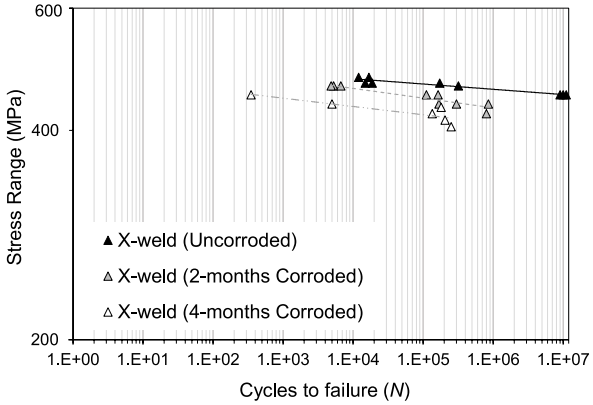

Fig. 5. Stress range (MPa) versus number of cycles to failure (*N*) for S355 cross-weld data tested at $R = 0.1$ with uncorroded and corroded condition.

The coefficient of determination, R^2, obtained from the lines of best fit made to the uncorroded, 2-months corroded, and 4-months corroded test data in Fig. 5 are found to be 0.90, 0.88 and 0.73, respectively. This indicates that due to the stochastic morphology of corrosion pits, the level of scatter in the corroded test data is higher than the uncorroded material, and the data distribution gets more scattered along with the exposure to seawater time, and hence severity of pitting corrosion increases. Furthermore, the presented data in Fig. 5 suggest that for each material state, the level of scatter can also change with the applied stress level. The general observation using the limited data on each material state reveal that the fatigue life scatter increases as the applied stress decreases, particularly in corroded samples. This is due to the fact that in higher stress fatigue tests, the surface condition is less likely to influence crack nucleation as micro-cracks are formed much earlier in the fatigue life, which is followed by crack growth. As a result, the variation in fatigue life is relatively small at higher stress levels for the material data sets examined in this study. On the other hand, at lower applied stress levels, the surface condition becomes more influential, and crack nucleation more heavily depends on small surface irregularities. Due to the unpredictable distribution of corrosion pits morphology, the influence of surface conditions becomes more pronounced at lower stress.

The trend seen in Fig. 5 can be explained by the shape of the pits. After shorter periods of corrosion time, the pit shapes were almost spherical while at longer periods these became elongated into cracks. Evidently the first effect of corrosion is to produce numerous pits, mostly hemispherical [21]. However, if one the pits is deeper than the neighbouring pits, the potential difference would cause an anodic point, which is the stressed region at the bottom of the pit and the cathode, which is the outer surface of the sample [25]. This will result in an extra corrosion damage that will sharpen and deepen the crack, thus producing further stress intensification and further raising the potential difference. Nevertheless, when the crack tip becomes very deep, the resistance between the anode and cathode will overcome the potential difference and some of the neighbouring pits in turn start to grow deeper [18,21]. When the corrosion stage is terminated or when the samples were taken out of the corrosive media and the lead crack has already grown, the stress concentration will already be considerable, and the subsequent fatigue life will be short, as can be seen in Fig. 5.

3.2. Influence of corrosion exposure time on fatigue life

In order to examine the time dependency of fatigue life on corrosion time, the number of cycles to failure in log-axis is plotted against the duration of seawater exposure time (i.e. 0, 2 and 4 months) in Fig. 6 at multiple values of stress range. It can be seen in Fig. 5 that for the highest value of stress range ($\Delta\sigma = 464$ MPa) considered in the analysis, there is a linear correlation between Log(N) (i.e. number of cycles to failure in log scale) and the seawater exposure time, indicating that the fatigue life at longer exposure times can be accurately predicted by performing shorter term tests with smaller seawater exposure times and extrapolating the linear correlation in "Log(N) vs. corrosion time" trend to longer corrosion times. The comparison of the trends in Fig. 6 reveals that this observation is valid only at high stress levels and as the value of stress range reduces, the correlation in "Log(N) vs. corrosion time" trend becomes non-linear. Finally seen in Fig. 6 is that the employment of a linear trend, as opposed to non-linear trend, for lower stress data would result in significant underprediction of the fatigue life at longer seawater exposure times and hence considerably higher level of conservatism in design and life prediction of offshore steel structures.

3.3. Fatigue life estimation model for corroded material

As shown in previous studies, it is known that in corroded steel structures, the cracks almost immediately initiate around corrosion pits and propagate when they reach the threshold stress intensity factor until failure occurs under Mode I [26]. In the present study, a simplified model has been proposed based on the equivalent initial flaw size (EIFS) approach by reverse engineering the S–N data and linking them to the experimentally determined size of the corrosion pits. The total fatigue life of a component comprises of two stages: the time for crack initiation and subsequent crack growth until failure occurs. The use of fracture mechanics to predict crack growth is well-developed and generally accurate. However, estimating the time for crack initiation remains challenging, as it depends on various

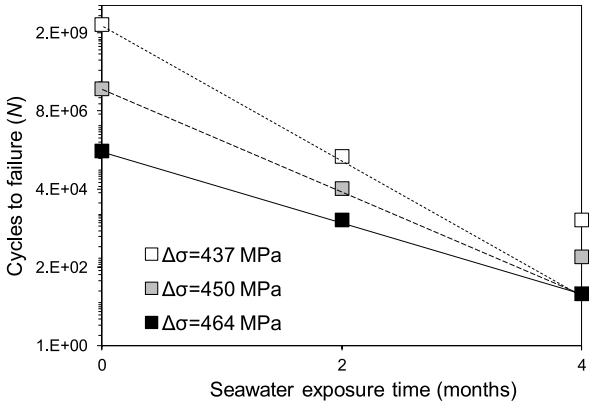

Fig. 6. Correlation of number of cycles to failure (N) with seawater exposure time at multiple stress levels.

factors such as material variability, machining effects, environment, stress concentrations, and loading history. There are two approaches which are commonly used to determine the Early Initiation of Fatigue Crack Growth. One approach assumes a "small crack" present from the beginning, continuously growing and is generally referred to as EIFS. The other approach assumes a specific time for crack initiation based on detectable sizes using non-destructive inspection (NDI) techniques [27,28]. In the present study the first approach has been employed and the measured corrosion pit has been assumed to be EIFS.

In this analysis the flaw around the pit geometry is assumed to be semi-elliptical surface crack to replicate the pitting corrosion and fatigue cracking mechanism in OWT support structures [8]. In order to calculate the stress intensity factor, K, of semi-elliptical surface crack, the aspect ratio a/c was taken to be less than one. The K solution was then calculated using the Newman-Raju formulae [29] shown in Equation (1)—(3).

$$K = \mathrm{S}\sqrt{\frac{\pi \mathrm{a}}{\mathrm{Q}}}\,\mathrm{F_s}\left(\frac{\mathrm{a}}{\mathrm{c}}, \frac{\mathrm{a}}{\mathrm{t}}, \frac{\mathrm{c}}{\mathrm{b}}, \varphi\right) \tag{1}$$

$$F_s = \left[\mathrm{M_1} + \mathrm{M_2}\left(\frac{a}{t}\right)^2 + \mathrm{M_3}\left(\frac{a}{t}\right)^4\right] g f_w f_\varnothing \tag{2}$$

$$Q = 1 + 1.464\left(\frac{a}{c}\right)^{1.65}, a/c < 1 \tag{3}$$

where S is the applied stress perpendicular to the crack plane, a the crack depth, c the crack length, b the width, t the thickness,φ the angular function, Q the shape factor and F_s the boundary correction factor the details of which can be found in Ref. [29].

The experimentally determined crack growth curves based on the EIFS approach can be described by Equation (4). Jones et al. [30] derived this equation from the original Hartman-Schijve equation and referred to it as a variant of the NASGRO equation [30–33]. The stress intensity factor range threshold, ΔK_{th}, asymptote was later included in the Forman equation by Hartman-Schijve [34] by changing the numerator to (ΔK - ΔK_{th}). A similar equation was also proposed by Priddle [35].

$$\frac{\mathrm{d}a}{\mathrm{d}N} = D\left(\frac{\Delta K - \Delta K_{\mathrm{thr}}}{\sqrt{1 - K_{\max}/A}}\right)^p \tag{4}$$

in Equation (4), K_{max} is the maximum value of stress intensity factor seen in a cycle, ΔK is the range of the stress intensity factor seen in a cycle and is defined as the difference between the maximum stress intensity factor K_{max} and minimum stress intensity factor K_{min}, ΔK_{thr} is the "effective fatigue threshold", A is the cyclic fracture toughness, and D and p are material constants. The term ΔK_{thr} in Equation (4) is derived from the ASTM E647 fatigue threshold ΔK_{th}, which is defined as the value of ΔK corresponding to a crack growth rate, da/dN, of equal to 10^{-10} m/cycle, using the following equation:

$$\Delta \mathrm{K_{th}} = \Delta \mathrm{K_{thr}} + \left(10^{-10}/\mathrm{D}\right)^{1/\mathrm{p}} \tag{5}$$

As illustrated in Refs. [27,33,36–40], it appears that the variability in crack growth can be modelled using the Hartman-Schijve crack growth equation [27,30]. In this work, Equation (4) was used to compute the variability in the crack growth history of S355 tests in air [6]. The calculated crack growth for S355 is shown in Fig. 7. The crack growth rate, da/dN, was plotted against $(\Delta K - \Delta K_{thr})/\sqrt{1 - K_{max}/A}$ in log-log axes as proposed and discussed in Refs. [37,38,41] where parameter A is the stress intensity factor range at fatigue failure. It is worth noting that in the threshold region, da/dN is not sensitive to the assumed A values in the range of 90–120 MPa $\sqrt{\mathrm{m}}$. The value of ΔK_{thr} was subsequently found using an iterative approach by employing the least squares method to make da/dN *vs.* $(\Delta K - \Delta K_{thr})/\sqrt{1 - K_{max}/A}$ plot in the near threshold region until it appears as a straight line as shown in Fig. 7(a). The

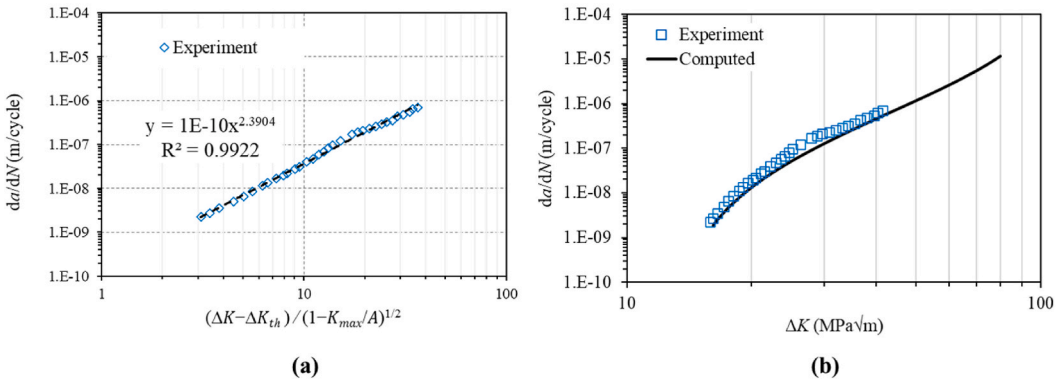

Fig. 7. Hartman-Schijve equation fitted to long crack test data: (a) for determining material constants D and p from the line of best fit, (b) comparison of the experimental and computed da/dN vs. ΔK crack growth data.

value of A was then adjusted to improve the linearity of the plot in the high ΔK region. This process generally results in negligible difference in the da/dN *vs.* $(\Delta K - \Delta K_{thr})/\sqrt{1 - K_{max}/A}$ plots in the high ΔK region. In this analysis, the value of A was estimated to be 120 MPa $\sqrt{\text{m}}$ and $\Delta K_{th} = 13$ MPa $\sqrt{\text{m}}$ [6].

A comparison between the experimentally measured and computed crack growth history for S355 test in air is shown in Fig. 7(b). The experimental data presented in this figure were taken from a previous study on the fatigue crack growth behaviour of S355 weldments by performing fracture mechanics tests on compact tension, C(T), specimens extracted from the same welded plate [10]. It can be seen that by allowing for variability in the fatigue threshold and the fracture toughness, reasonably good agreement was obtained between the experimental and computed results. The values of the parameters D and p used in this study are 1×10^{-10} and 2.39, respectively, which were found from the analysis shown in Fig. 7(a).

The *S–N* fatigue life for corroded material examined in this study was then calculated by numerical integration of Equation (4) using material constants identified in Fig. 7(a). Due to the higher population of data points for 2-months corroded samples compared to 4-months corroded data set, the *S–N* curve prediction was made for 2-months corroded samples at different values of stress range to demonstrate the capability of the model. In order to keep the model simple, the following assumptions were made in the analysis: (i) Fatigue life estimations are based on LEFM formulation, (ii) Fatigue crack initiation is neglected hence the corrosion pit is treated as an initial crack, (iii) Fatigue crack propagation of short crack is neglected.

Fig. 8 shows the comparison of the predicted *S–N* data for 2-months corroded material with test experimental data set. In this analysis, the initial crack length for 2-months corroded samples was taken as 0.1 mm which was obtained from XCT conducted on the test specimens, an example of which is shown in Fig. 8. As seen in the XCT result, the analysis of the corroded samples revealed that the corrosion pits appeared on the outer surface of immersed samples were less than 0.1 mm deep hence the pit size is negligible compared to the specimen thickness and the cross-sectional area can be assumed to remain unchanged in the *S–N* fatigue analysis. The results in Fig. 8 show considering the inherent experimental scatter particularly in fatigue behaviour of corroded material, acceptable mean *S–N* life prediction is made using the EIFS approach and the predicted line falls within and almost in the middle of the cloud of data from 2-months corroded samples; however, it is evident that the predicted line cannot provide the design *S–N* curve by considering the worst-case scenario in the fatigue response of pitted material. In other words, by taking into account the high level of scatter in fatigue data from corroded samples, the results show that an acceptable fit can be obtained from the analysis conducted in this study; however, this model cannot predict the upper bound and lower bound data scatters which often appear in the experimental data.

It must be noted that the influence of corrosion pits on the fatigue performance has been found to be substantial and the pitting morphology is heavily dependent on seawater exposure time (i.e., either two months or four months in this study). According to the results obtained from the EIFS approach, the lower fatigue life of 4-months corroded samples can be attributed to larger size of the corrosion pits which results in higher stress concentrations hence faster crack propagation. The results from this study show that the effect of corrosion pits on subsequent fatigue life can be predicted using the EIFS approach; however, further extensive validations with short crack data and pit morphology characterisation need to be performed in future work to improve the accuracy level of prediction in highly scattered data obtained from corroded steel samples.

Moreover, due to the stochastic nature of pitting corrosion which makes it extremely difficult to predict the pit size and density, a probabilistic-based methodology needs to be adopted in conjunction with the EIFS approach to account for the variability in the pit/initial crack size and its subsequent effect on the level of scatter in the predicted *S–N* curve. This need to be conducted in future work work to predict the *S–N* behaviour of longer-term corroded material with higher level of confidence. Having said that, in the absence of the large number of data points and probability-based approach, it appears that the prediction made with the simple EIFS approach provides an acceptable estimate of the *S–N* fatigue behaviour of the corroded material. However, this prediction cannot be used for design purposes and significant effort needs to be put in future work to predict the lower bound *S–N* fatigue behaviour (i.e. mean-2SD) of corroded material using a probability-based approach.

4. Conclusions

The influence of pitting corrosion on the *S–N* fatigue life of S355 cross-weld specimens was experimentally determined and a predictive fracture mechanics-based model was developed to carry out the durability analysis. Moreover, the influence of seawater exposure time on the fatigue life of the material was critically evaluated at different stress levels. The fatigue samples were initially immersed in artificial seawater for different durations of 0, 2 and 4 months and subsequently tested in air at different stress levels with the load ratio of 0.1 and frequency of 20 Hz. The results from this study show that pitting corrosion significantly decreases the fatigue life of the material and for a given value of stress range the level of fatigue life reduction increases by increasing the seawater exposure time. Moreover, the lines of best fit made to the *S–N* fatigue data show that similar slopes are obtained for corroded and uncorroded data sets implying that the indicative fatigue endurance limit would continuously decrease as the seawater exposure time and population of corrosion pits increase in the material. The analysis of the corroded samples showed that when Log(N) data is plotted against the seawater exposure time, a linear trend can be observed at high stress levels which will gradually transform into a non-linear trend at lower stress levels. Finally, it was shown that the durability of the corroded material can be predicted in the form of mean *S–N* curve using the fracture mechanics approach by employing the modified Hartman-Schijve equation and the equivalent initial flaw size (EIFS) as the initial crack length.

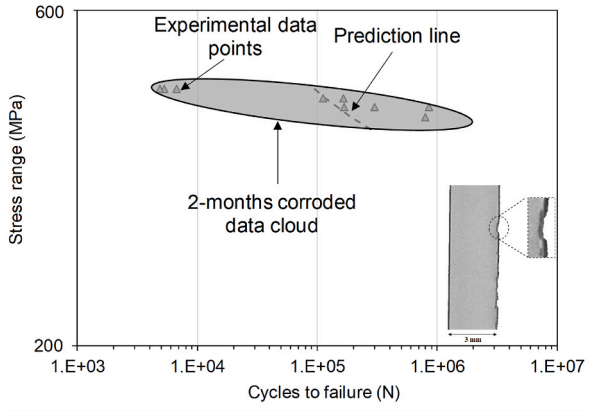

Fig. 8. Compared of the predicted *S–N* curve for 2-months corroded samples with the experimental data.

Declaration of competing interest

The authors declare that they have no known competing financial interests or personal relationships that could have appeared to influence the work reported in this paper.

Data availability

Data will be made available on request.

Acknowledgements

This work was supported by the Supergen ORE Hub Flexible Funding under grant number EP/S000747/1 from the UK Engineering and Physical Sciences Research Council (EPSRC). The author would like to acknowledge the help from Andrea Giampiccolo for contribution to fatigue testing in the structural integrity laboratory.

References

[1] Johnston B, Foley A, Doran J, Littler T. Levelised cost of energy, A challenge for offshore wind. Renew Energy 2020;160:876–85. https://doi.org/10.1016/j.renene.2020.06.030.
[2] Jacob A, Oliveira J, Mehmanparast A, Hosseinzadeh F, Kelleher J, Berto F. Residual stress measurements in offshore wind monopile weldments using neutron diffraction technique and contour method. Theor Appl Fract Mech 2018;96:418–27. https://doi.org/10.1016/j.tafmec.2018.06.001.
[3] Dorell G, Diaz V. Siemens Gamesa's flagship 14 MW turbine to power 1.4 GW Sofia offshore wind power project in the UK. Renew Energy 2020. https://www.siemensgamesa.com/en-int/newsroom/2020/06/20200620-siemens-gamesa-press-release-offshore-sofia-uk.
[4] Offshore wind operational report 2020. 2020.
[5] Dirisu P, Supriyo G, Martina F, Xu X, Williams S. Wire plus arc additive manufactured functional steel surfaces enhanced by rolling. Int J Fatig 2020;130. https://doi.org/10.1016/j.ijfatigue.2019.105237.
[6] Mehmanparast A, Brennan F, Tavares I. Fatigue crack growth rates for offshore wind monopile weldments in air and seawater : SLIC inter-laboratory test results. JMADE 2017;114:494–504. https://doi.org/10.1016/j.matdes.2016.10.070.
[7] Biswal R. On the performance of monopile weldments under service loading conditions and fatigue damage prediction. 2021. p. 1469–83. https://doi.org/10.1111/ffe.13442.
[8] Bocher M, Mehmanparast A, Braithwaite J, Shafiee M. New shape function solutions for fracture mechanics analysis of offshore wind turbine monopile foundations. Ocean Eng 2018;160:264–75. https://doi.org/10.1016/j.oceaneng.2018.04.073.
[9] Arany L, Bhattacharya S, Macdonald J, Hogan SJ. Design of monopiles for offshore wind turbines in 10 steps. Soil Dynam Earthq Eng 2017;92:126–52. https://doi.org/10.1016/j.soildyn.2016.09.024.
[10] Jacob A, Mehmanparast A, D'Urzo R, Kelleher J. Experimental and numerical investigation of residual stress effects on fatigue crack growth behaviour of S355 steel weldments. Int J Fatig 2019;128:105196. https://doi.org/10.1016/j.ijfatigue.2019.105196.
[11] Mehmanparast A, Taylor J, Brennan F, Tavares I. Experimental investigation of mechanical and fracture properties of offshore wind monopile weldments: SLIC interlaboratory test results. Fatig Fract Eng Mater Struct 2018;41:2485–501. https://doi.org/10.1111/ffe.12850.
[12] Igwemezie V, Mehmanparast A. Waveform and frequency effects on corrosion-fatigue crack growth behaviour in modern marine steels. Int J Fatig 2020;134:105484. https://doi.org/10.1016/j.ijfatigue.2020.105484.
[13] Igwemezie V, Mehmanparast A, Brennan F. The role of microstructure in the corrosion-fatigue crack growth behaviour in structural steels. Mater Sci Eng 2021;803:140470. https://doi.org/10.1016/j.msea.2020.140470.
[14] Colussi M, Ferro P, Berto F, Meneghetti G. In: Ferro P, Berto F, editors. Rapid calculation of residual notch stress intensity factors (R- NSIFs) by means of the peak stress method. Rijeka: IntechOpen; 2018. https://doi.org/10.5772/intechopen.73514. Ch. 7.
[15] Ferro P, Berto F, James MN. Asymptotic residual stresses in butt-welded joints under fatigue loading. Theor Appl Fract Mech 2016;83:114–24. https://doi.org/10.1016/j.tafmec.2016.02.002.
[16] Shojai S, Schaumann P, Braun M. Influence of pitting corrosion on the fatigue strength of offshore steel structures based on 3D surface scans. 2022. p. 164. https://doi.org/10.1016/j.ijfatigue.2022.107128.
[17] Farhad F. Fatigue of X65 steel in the sour corrosive environment — a novel experimentation and analysis method for predicting fatigue crack initiation life from corrosion pits. 2021. p. 1195–208. https://doi.org/10.1111/ffe.13423.

[18] Larrosa NO, Akid R, Ainsworth RA. Corrosion-fatigue: a review of damage tolerance models. Int Mater Rev 2018;63:283–308. https://doi.org/10.1080/09506608.2017.1375644.
[19] Qvale P, Zarandi EP, Ås SK, Skallerud BH. Digital image correlation for continuous mapping of fatigue crack initiation sites on corroded surface from offshore mooring chain. Int J Fatig 2021;151. https://doi.org/10.1016/j.ijfatigue.2021.106350.
[20] Melchers RE. A review of trends for corrosion loss and pit depth in longer-term exposures. 2018. p. 42–58. https://doi.org/10.3390/cmd1010004.
[21] Winston Revie R, Herbert H U. Alloying for corrosion resistance; stainless steels. In: Corrosion and corrosion control; 2008. p. 333–65. https://doi.org/10.1002/9780470277270.ch19.
[22] Li L, Mahmoodian M, Li C-Q, Robert D. Effect of corrosion and hydrogen embrittlement on microstructure and mechanical properties of mild steel. Construct Build Mater 2018;170:78–90. https://doi.org/10.1016/j.conbuildmat.2018.03.023.
[23] ASTM-E466. Standard practice for conducting force controlled constant amplitude axial fatigue tests of metallic materials. Test 2002;3:4–8. https://doi.org/10.1520/E0466-07.2.
[24] ASTM-D1141. Standard Practice for Preparation of Substitute Ocean Water 2021;1(50):7–9. https://doi.org/10.1520/D1141-98R21.2.
[25] Gough J. The mechanism of corrosion fatigue of mild steel. 1935. p. 372–92.
[26] Farhad F, Smyth-Boyle D, Zhang X. Fatigue of X65 steel in the sour corrosive environment—a novel experimentation and analysis method for predicting fatigue crack initiation life from corrosion pits. Fatig Fract Eng Mater Struct 2021;44:1195–208. https://doi.org/10.1111/ffe.13423.
[27] Jones R. Fatigue crack growth and damage tolerance. Fatig Fract Eng Mater Struct 2014;37:463–83. https://doi.org/10.1111/ffe.12155.
[28] Johnson WS. Procedia Engineering the history , logic and uses of the Equivalent Initial Flaw Size approach to total fatigue life prediction. Procedia Eng 2010;2:47–58. https://doi.org/10.1016/j.proeng.2010.03.005.
[29] Newman Jr JC, Raju IS. Stress-intensity factor equations for cracks in three-dimensional finite bodies, vol. 1. ASTM Special Technical Publication; 1983. p. 238–65. https://doi.org/10.1520/stp37074s.
[30] Jones R, Molent L, Walker K. Fatigue Crack Growth in a Diverse Range of Materials 2012;40:43–50. https://doi.org/10.1016/j.ijfatigue.2012.01.004.
[31] Molent L, Jones R. The influence of cyclic stress intensity threshold on fatigue life scatter. Int J Fatig 2016;82:748–56. https://doi.org/10.1016/j.ijfatigue.2015.10.006.
[32] Jones R, Raman RKS, Iliopoulos AP, Michopoulos JG, Phan N, Peng D. Additively manufactured Ti-6Al-4V replacement parts for military aircraft. Int J Fatig 2019;124:227–35. https://doi.org/10.1016/j.ijfatigue.2019.02.041.
[33] Iliopoulos A, Jones R, Michopoulos J, Phan N, Singh Raman R. Crack growth in a range of additively Manufactured aerospace structural materials. Aerospace 2018;5:118. https://doi.org/10.3390/aerospace5040118.
[34] Hartman A, Schijve J. The effects of environment and load frequency on the crack propagation law for macro fatigue crack growth in aluminium alloys. Eng Fract Mech 1970;1:615–31. https://doi.org/10.1016/0013-7944(70)90003-2.
[35] Priddle E. High cycle fatigue crack propagation under random and constant amplitude loadings. Int J Pres Ves Pip 1976;4:89–117.
[36] Shamir M, Igwemezie V, Lotfian S, Asif H, Ganguly S, Mehmanparast A. Assessment of mechanical and fatigue crack growth properties of wire + arc additively manufactured mild steel components. 2022. p. 2978–89. https://doi.org/10.1111/ffe.13797.
[37] Shamir M, Zhang X, Syed AK. Characterising and representing small crack growth in an additive manufactured titanium alloy. Eng Fract Mech 2021;253:107876. https://doi.org/10.1016/j.engfracmech.2021.107876.
[38] Jones R, Michopoulos JG, Iliopoulos AP, Singh Raman RK, Phan N, Nguyen T. Representing crack growth in additively manufactured Ti-6Al-4V. Int J Fatig 2018;116:610–22. https://doi.org/10.1016/j.ijfatigue.2018.07.019.
[39] Jones R, Rans C, Iliopoulos AP, Michopoulos JG, Phan N, Peng D. Modelling the variability and the anisotropic behaviour of crack growth in slm ti-6al-4v. Materials 2021;14. https://doi.org/10.3390/ma14061400.
[40] Jones R, Kovarik O, Cizek J, Ang A, Lang J. Crack growth in conventionally manufactured pure nickel, titanium and aluminum and the cold spray additively manufactured equivalents. Addit Manuf Lett 2022:100043. https://doi.org/10.1016/j.addlet.2022.100043.
[41] Iliopoulos AP, Jones R, Michopoulos JG, Phan N, Rans C. Further studies into crack growth in additively manufactured materials. Materials 2020;13:5–10. https://doi.org/10.3390/ma13102223.

Fatigue life assessment of offshore wind support structures in the presence of corrosion pits

Shamir, Muhammad

2023-11-01

Shamir M, Braithwaite J, Mehmanparast A. (2023) Fatigue life assessment of offshore wind support structures in the presence of corrosion pits. Marine Structures, Volume 92, November 2023, Article Number 103505

https://doi.org/10.1016/j.marstruc.2023.103505